THE JOURNAL OF BIOLOGICAL CHEMISTRY VOL. 290, NO. 13, pp. 8582–8590, March 27, 2015

How pH Modulates the Dimer-Decamer Interconversion of 2-Cys Peroxiredoxins from the Prx1 Subfamily*

Received for publication, October 21, 2014, and in revised form, January 29, 2015 Published, JBC Papers in Press, February 9, 2015, DOI 10.1074/jbc.M114.619205

Mariana A. B. Morais[‡1], Priscila O. Giuseppe[‡1], Tatiana A. C. B. Souza[§], Thiago G. P. Alegria[¶], Marcos A. Oliveira[‖], Luis E. S. Netto[¶], and Mario T. Murakami[‡2]

From the [‡]Laboratório Nacional de Biociências, Centro Nacional de Pesquisa em Energia e Materiais, Campinas/SP, 13083-970, the [§]Laboratório de Proteômica e Engenharia de Proteínas, Instituto Carlos Chagas, Fiocruz, Curitiba/PR, 81350-010, the [¶]Departamento de Genética e Biologia Evolutiva, Instituto de Biociências, Universidade de São Paulo, São Paulo/SP, 05508-900, and the [‖]Departamento de Biologia, Universidade Estadual Paulista Júlio de Mesquita Filho, Campus do Litoral Paulista, São Vicente/SP 11330-900, Brazil

Background: Oligomeric changes affect the function of typical 2-Cys peroxiredoxins.
Results: pH decrease favors decamerization and this effect depends on His^{113} and Asp^{76}.
Conclusion: Protonated His^{113} attracts Asp^{76} inducing a conformational change that stabilizes the decamer.
Significance: Learning how pH modulates the oligomerization of typical 2-Cys peroxiredoxins is an important step into understanding the pH effect on their function.

2-Cys peroxiredoxins belonging to the Prx1 subfamily are Cys-based peroxidases that control the intracellular levels of H_2O_2 and seem to assume a chaperone function under oxidative stress conditions. The regulation of their peroxidase activity as well as the observed functional switch from peroxidase to chaperone involves changes in their quaternary structure. Multiple factors can modulate the oligomeric transitions of 2-Cys peroxiredoxins such as redox state, post-translational modifications, and pH. However, the molecular basis for the pH influence on the oligomeric state of these enzymes is still elusive. Herein, we solved the crystal structure of a typical 2-Cys peroxiredoxin from *Leishmania* in the dimeric (pH 8.5) and decameric (pH 4.4) forms, showing that conformational changes in the catalytic loop are associated with the pH-induced decamerization. Mutagenesis and biophysical studies revealed that a highly conserved histidine (His^{113}) functions as a pH sensor that, at acidic conditions, becomes protonated and forms an electrostatic pair with Asp^{76} from the catalytic loop, triggering the decamerization. In these 2-Cys peroxiredoxins, decamer formation is important for the catalytic efficiency and has been associated with an enhanced sensitivity to oxidative inactivation by overoxidation of the peroxidatic cysteine. In eukaryotic cells, exposure to high levels of H_2O_2 can trigger intracellular pH variations, suggesting that pH changes might act cooperatively with H_2O_2 and other oligomerization-modulator factors to regulate the structure and function of typical 2-Cys peroxiredoxins in response to oxidative stress.

Peroxiredoxins (Prxs)[3] are key components for antioxidant protection and cell signaling pathways (1). They are classified into distinct subfamilies, according to their active site architecture and sequence similarity (2). The Prx1 subfamily comprises typical 2-Cys Prxs that are highly expressed and found in all living kingdoms (3). In eukaryotes, Prx1 subfamily members are present not only in the cytosol (4, 5) but also in organelles such as mitochondrion (4, 6), chloroplast (7), and endoplasmic reticulum (8). This subfamily includes the bacterial AhpC proteins, the human Prxs I to IV, the yeast thiol-specific antioxidant protein, and the tryparedoxin peroxidases (3).

Prx1 subfamily members are obligate homodimers that display two identical active sites located in opposite sides of the dimer interface (9). In most cases, Prx1 homodimers can associate noncovalently forming doughnut-like assemblies that are usually decameric (3). The dimer-decamer interconversion seems to play a role during the catalytic cycle, influencing the catalytic efficiency (10). Some studies support that Prx1 subfamily members can further form higher-order oligomers, which seems to switch their function from peroxidase to chaperone (11, 12).

The redox state of the peroxidatic cysteine (C_P) is the best characterized factor regulating the oligomerization of Prx1 subfamily members (10, 13). When C_P is reduced, the catalytic loop and C-terminal extension adopt a fully folded (FF) conformation, which stabilizes the decameric form. By reducing peroxides (ROOH) to ROH, C_P is oxidized to sulfenic acid (C_P-SOH) and the active site becomes locally unfolded (LU), allowing the formation of a disulfide bond between C_P-SOH and the resolving cysteine (C_R), located in the other subunit forming the catalytic interface (3). This conformational change favors the dissociation of decam-

* This work was supported by Fundação de Amparo à Pesquisa do Estado de São Paulo (FAPESP) Grants 2010/51730-0, 2011/10248-4, and 2012/24134-3, the Conselho Nacional de Desenvolvimento Científico e Tecnológico (CNPq), and the Coordenação de Aperfeiçoamento de Pessoal de Nível Superior (CAPES).
[1] Both authors contributed equally to this work.
[2] To whom correspondence should be addressed. Tel.: 55-19-3512-1106; Fax: 55-19-3512-1100; E-mail: mario.murakami@lnbio.cnpem.br.

[3] The abbreviations used are: Prx, peroxiredoxin; aSEC, analytical size-exclusion chromatography; C_P, peroxidatic cysteine; C_P-loop, catalytic loop; C_R, resolving cysteine; DLS, dynamic light scattering; DTNB, 5,5′-dithiobis-(2-nitrobenzoic acid); FF, fully folded; *Lb*Prx1m, mitochondrial tryparedoxin peroxidase from *Leishmania braziliensis*; LU, locally unfolded; R_H, hydrodynamic radius; TEV, tobacco etch virus.

ers into dimers (10, 13). Under oxidative stress, some Prx1 subfamily members can be inactivated by C_P overoxidation and assume higher-order oligomeric states that display chaperone function as shown *in vitro* (11, 12, 14).

Besides the redox state, other factors such as post-translational modifications, ionic strength, and pH can also affect the equilibrium of Prx1 oligomers (15). For the human Prx I, phosphorylation of Thr^{90} triggers the formation of high molecular weight complexes and seems to induce the functional switch to chaperone (16), whereas Cys^{83} glutathionylation (17) and Cys^{52} nitrosylation (18) favor decamer dissociation. The ionic strength seems to have opposing effects depending on the Prx1 subfamily member. High ionic strength (>0.3 M NaCl) stabilizes the decameric form of Prx1 members from plant and bacteria, but favors the dimeric form of the rat Prx I (7, 19, 20). Acidification favors the decameric state of plant and mammalian Prx1 subfamily members (7, 21). The dimer-decamer equilibrium of these enzymes is highly responsive to small pH variations in the physiological range (between pH 7 and 8), suggesting that a dissociable group with a pK_a value in this pH interval affects the equilibrium between the two oligomeric states (7, 21).

Intracellular pH variations play an important and underappreciated role in physiological and pathological situations such as apoptosis, neurotransmission, and insulin secretion in mammals as well as CO_2 fixation in plants (22, 23). It has been shown that such pH variations can modulate the structure and function of proteins, including caspases (22, 24) and enzymes belonging to the Prx1 subfamily (7). Nevertheless, the molecular mechanisms by which pH controls Prx1 oligomerization remain elusive.

Therefore, we investigated the structural basis for the pH-dependent decamerization of Prx1 subfamily members using as a model the mitochondrial tryparedoxin peroxidase from *Leishmania braziliensis*, here named *Lb*Prx1m according to the nomenclature proposed by Gretes *et al.* (25). Up-regulation of this protein has been associated with protection against apoptosis-like death (26) and resistance to miltefosine (27), a drug whose activity is linked to apoptosis and disturbance of lipid-dependent cell signaling pathways (28). Moreover, *Leishmania* Prx1m confers thermotolerance to the parasite and displays *in vitro* chaperone activity, which seems to be crucial for virulence (29). In this work, we solved the crystal structure of *Lb*Prx1m at basic and acidic conditions, providing, for the first time to our knowledge, structural data of a Prx1 subfamily member in both dimeric and decameric states induced by pH variations. Structural comparisons along with site-directed mutagenesis and biophysical studies revealed that His^{113} functions as a pH sensor. With decreasing pH, His^{113} becomes protonated and attracts Asp^{76}, inducing a conformational change in the catalytic loop that promotes the decamerization. The ionic pair, His^{113} and Asp^{76}, is present in most Prx1 subfamily members, suggesting that this mechanism is conserved in typical 2-Cys Prxs.

EXPERIMENTAL PROCEDURES

Molecular Cloning and Site-directed Mutagenesis—The *Lb*Prx1m gene (RefSeq XM_001562186.1) was cloned into a pET28a-His-TEV vector between NdeI and SalI restriction sites as described in Ref. 30. The $Asp^{76} \rightarrow$ Ala and $His^{113} \rightarrow$ Ala mutants were produced using the QuikChange™ site-directed mutagenesis kit (Stratagene).

Protein Expression and Purification—The wild-type (wt) *Lb*Prx1m and mutants were expressed in *Escherichia coli* BL21(*DE3*)Δ*SlyD* cells harboring plasmid pRARE2 as described (30). For protein purification, cells were resuspended in buffer A (20 mM sodium phosphate, pH 7.4, 500 mM NaCl, and 5 mM imidazole) containing 2 mM PMSF, disrupted by sonication and centrifuged at 20,000 × *g* for 30 min (277 K). The supernatant was loaded onto a nickel-charged Hi-trap chelating column (5 ml, GE Healthcare) coupled to an Akta FPLC system (GE Healthcare). After washing the resin with 10 column volumes of buffer A, bound proteins were eluted using a non-linear imidazole gradient from 5 to 1000 mM. Fractions containing the target protein were dialyzed against 25 mM Tris-HCl (pH 7.5) and loaded onto a Q-Sepharose Fast Flow column (5 ml, GE Healthcare). The target protein was eluted with 0.15 M NaCl during a 0–1 M NaCl gradient. The fractions were pooled, concentrated, and subjected to a size-exclusion chromatography using a HiLoad 16/600 Superdex 200 column (GE Healthcare) pre-equilibrated with 25 mM Tris-HCl (pH 7.5). The protein was purified and analyzed under non-reducing conditions, unless otherwise stated. The oxidation state of samples was verified by SDS-PAGE under reducing and non-reducing conditions.

Analytical Size Exclusion Chromatography (aSEC)—Analytical SEC experiments at different pH values were carried out on a Superdex 200 10/300 GL column (GE Healthcare) using a flow rate of 0.5 ml min^{-1}. *Lb*Prx1m samples, previously incubated with the Chelex® 100 resin (Bio-Rad), were diluted to 48 μM using the respective aSEC buffers and loaded onto the column pre-equilibrated with 50 mM MMT (DL-malic acid, MES, and Tris base), pH values of 4, 5, 6, 7, or 8, 150 mM NaCl, and 10 mM EDTA. The D76A and H113A mutants (48 μM), previously incubated at pH 4.0 (50 mM MMT, pH 4, 150 mM NaCl, 10 mM EDTA) or at pH 7.0 with DTT (25 mM Tris-HCl, pH 7.0, 150 mM NaCl, 5 mM EDTA, and 2 mM DTT) by 30 min, were loaded onto the column pre-equilibrated with the corresponding buffers. To evaluate whether the N-terminal His tag and the protein redox state influence the pH effect on the dimer-to-decamer conversion, the same assay was performed with *Lb*Prx1m pre-treated with TEV protease. For the cleavage, *Lb*Prx1m at 1 mg ml^{-1} was treated with His-tagged TEV protease (0.01 mg ml^{-1}) for 30 min at 298 K. The samples were loaded onto a nickel-nitrilotriacetic acid Superflow resin (Qiagen) to separate the cleaved protein (collected from the flow-through) from the remaining uncleaved *Lb*Prx1m and His-tagged TEV protease. Analytical SEC runs were performed in the presence and absence of 2 mM DTT, in 25 mM Tris-HCl (pH 7.0, 7.5, and 8.0) containing 150 mM NaCl and 5 mM EDTA. All these experiments were carried out under chelating conditions because some divalent cations stabilize the *Lb*Prx1m decamer at alkaline pH values.[4] The SEC column was calibrated using low and high molecular weight markers (GE Healthcare).

[4] M. A. B. Morais, P. O. Giuseppe, T. A. C. B. Souza, T. G. P. Alegria, M. A. Oliveira, L. E. S. Netto, and M. T. Murakami, unpublished data.

Quantification of Free Thiol Groups—*Lb*Prx1m samples (48 μM) in 25 mM Tris-HCl (pH 7.5), 150 mM NaCl, and 5 mM EDTA were treated with 2 mM DTT for 30, 60, 120, and 240 min at room temperature. Excess DTT was removed using the HiTrap Desalting column (5 ml, GE Healthcare). The samples were incubated with 100 μM DTNB for 1 h. The 2-nitro-5-thiobenzoate production was monitored spectrophotometrically at 412 nm ($\epsilon_{412} = 14{,}150\ M^{-1}\ cm^{-1}$) and the eluted protein concentrations were used to calculate the number of free thiols per molecule.

Dynamic Light Scattering (DLS)—DLS measurements were performed under non-reducing conditions on a Dynapro Molecular Sizing instrument at 291 K. Protein samples at 48 μM were previously centrifuged for 20 min at 20,000 $\times$ *g*. Data were collected with intervals of 10 s with at least 100 acquisitions. The diffusion coefficient (D) was determined from the analysis of measured time-dependent fluctuations in the scattering intensity and used to calculate the hydrodynamic radius (R_H) of the protein via Stokes-Einstein equation. Data analysis was performed using the software Dynamics V6.3.40.

Crystallization, Data Collection, Processing, and Structure Determination—*Lb*Prx1m sample was concentrated to 10 mg ml^{-1} for crystallization trials. Crystals of the dimeric form were grown by the sitting-drop vapor-diffusion method in drops containing 0.5 μl of the protein sample mixed with an equal volume of reservoir solution (27% (w/v) PEG4000, 0.1 M Tris-HCl, pH 8.5, 0.2 M Li_2SO_4) added by 5 mM EDTA at 291 K. The decameric form was crystallized in 0.1 M MMT buffer (pH 4.4), 13.9% (w/v) PEG1500, and 25 mM $CaCl_2$ by the hanging drop method in drops containing 2 μl of protein and 1 μl of mother liquor at 291 K.

X-ray diffraction data were collected at the W01B-MX2 beamline (LNLS, Campinas, Brazil). Data were indexed, integrated, merged, and scaled using HKL2000 (31) or XDS (32). Structures were solved by molecular replacement using the atomic coordinates of Hbp23 (PDB code 1QQ2, 60% sequence identity) as template and the program MOLREP (33) for the dimer or PHASER (34) and PHENIX AutoBuild Wizard (35) for the decamer. Model refinement was carried out alternating cycles of REFMAC5 (36) or phenix.refine (37), with visual inspection of the electron density maps and manual rebuilding with COOT (38). Refinement cycles included non-crystallographic symmetry, secondary structure, and reference model restraints as well as translation/libration/screw parameters from the TLSMD server (39). The model quality was assessed using MolProbity (40). Data collection and refinement statistics are shown in Table 1. Dimeric and decameric *Lb*Prx1m structures were deposited in the RCSB Protein Data Bank under accession codes 4KCE and 4KB3, respectively.

TABLE 1
Data collection and refinement statistics

	Decamer	Dimer
Data collection		
Space group	$P2_12_12_1$	$P4_22_12$
Cell dimensions		
a, *b*, *c* (Å)	90.2, 98.9, 228.1	132.5, 132.5, 44.6
Molecules per AU[a]	10	2
Resolution (Å)	40.0-2.9 (3.1-2.9)[b]	40.0-2.8 (3.0-2.8)
Observed reflections	397,953 (54,334)	137,931 (18,831)
Unique reflections	44,560 (6,943)	10,240 (1,506)
R_{merge} (%)	25.4 (219.5)	20.0 (322.1)
R_{meas} (%)	26.9 (234.8)	20.9 (335.5)
$I/\sigma I$	9.9 (0.9)	10.6 (0.9)
$CC_{1/2}$[c]	1.0 (0.5)	1.0 (0.5)
Completeness (%)	99.5 (97.6)	98.7 (92.9)
Multiplicity	9 (8)	13 (13)
Refinement		
Resolution (Å)	20.0-2.9	19.9-2.8
No. reflections	44,517	10,200
R_{work}/R_{free}	0.23/0.28	0.24/0.28
No. atoms		
Protein	12,942	2,592
Mean *B*-factors (Å^2)		
Protein	83	54
Root mean square deviations		
Bond lengths (Å)	0.006	0.007
Bond angles (°)	1.122	1.069
Ramachandran Plot		
Favored (%)	96.9	95.4
Allowed (%)	2.8	4.6
Disallowed (%)	0.3	0.0
Molprobity clashscore	10.4	5.8

[a] AU, asymmetric unit.
[b] Values in parentheses are for highest-resolution shell.
[c] $CC_{1/2}$, correlation between intensities from random half-datasets (51).

RESULTS

Acidification Shifts the Dimer-Decamer Equilibrium to the Decameric State—*Lb*Prx1m purified under non-reducing conditions assumes the disulfide-bonded state (SS), as shown by SDS-PAGE analysis (Fig. 1*A*). Analytical SEC experiments of this sample at different pH values revealed that decreasing pH induces the oxidized *Lb*Prx1m dimers to associate into decamers (Fig. 1*C*). At pH 8, *Lb*Prx1m was essentially dimeric, whereas at pH $\leq$ 7 *Lb*Prx1m was predominantly decameric, indicating that the decamer-to-dimer transition occurs in a narrow pH range between pH 7 and 8.

Corroborating the aSEC results, DLS measurements of oxidized *Lb*Prx1m (48 μM) at pH 8 and 4 indicate averaged R_H of 2.9 and 5.7 nm, respectively (Fig. 1*D*). These values are in agreement with the theoretical R_H estimated for the dimer (3.1 nm) and decamer (6.1 nm) based on the molecular mass of the respective oligomers (46 and 230 kDa).

To evaluate the influence of the protein redox state on this transition, we analyzed samples treated with 2 mM DTT (Fig. 1*F*). Under this condition, *Lb*Prx1m assumes a reduced state, according to SDS-PAGE analysis and thiol quantification (Fig. 1, *A* and *B*). The DTT-treated samples maintained a number of free thiols close to three, which is consistent with the number of cysteines of *Lb*Prx1m (Cys^{81}, Cys^{107}, and Cys^{204}).

Analytical SEC experiments with or without DTT were performed at different pH conditions using TEV-cleaved *Lb*Prx1m (without His tag) (Fig. 1, *E* and *F*). Unlike the mitochondrial Prx III (41), removal of the His tag did not influence the dimer-decamer equilibrium of oxidized *Lb*Prx1m. Regarding the reduced protein, it remained dimeric at pH 8 and decameric at pH 7, similarly to the oxidized form (Fig. 1, *E* and *F*). However, treatment with DTT increased the decameric fraction at pH 7, suggesting that, at this pH, reduced decamers are more stable than those oxidized. At pH 7.5, the oxidized protein remained predominantly dimeric, whereas those that were reduced eluted as a mixed population of dimers, intermediate species, and decamers. These results indicate that, at this pH, C_P reduction is not sufficient to fully convert dimers into decamers.

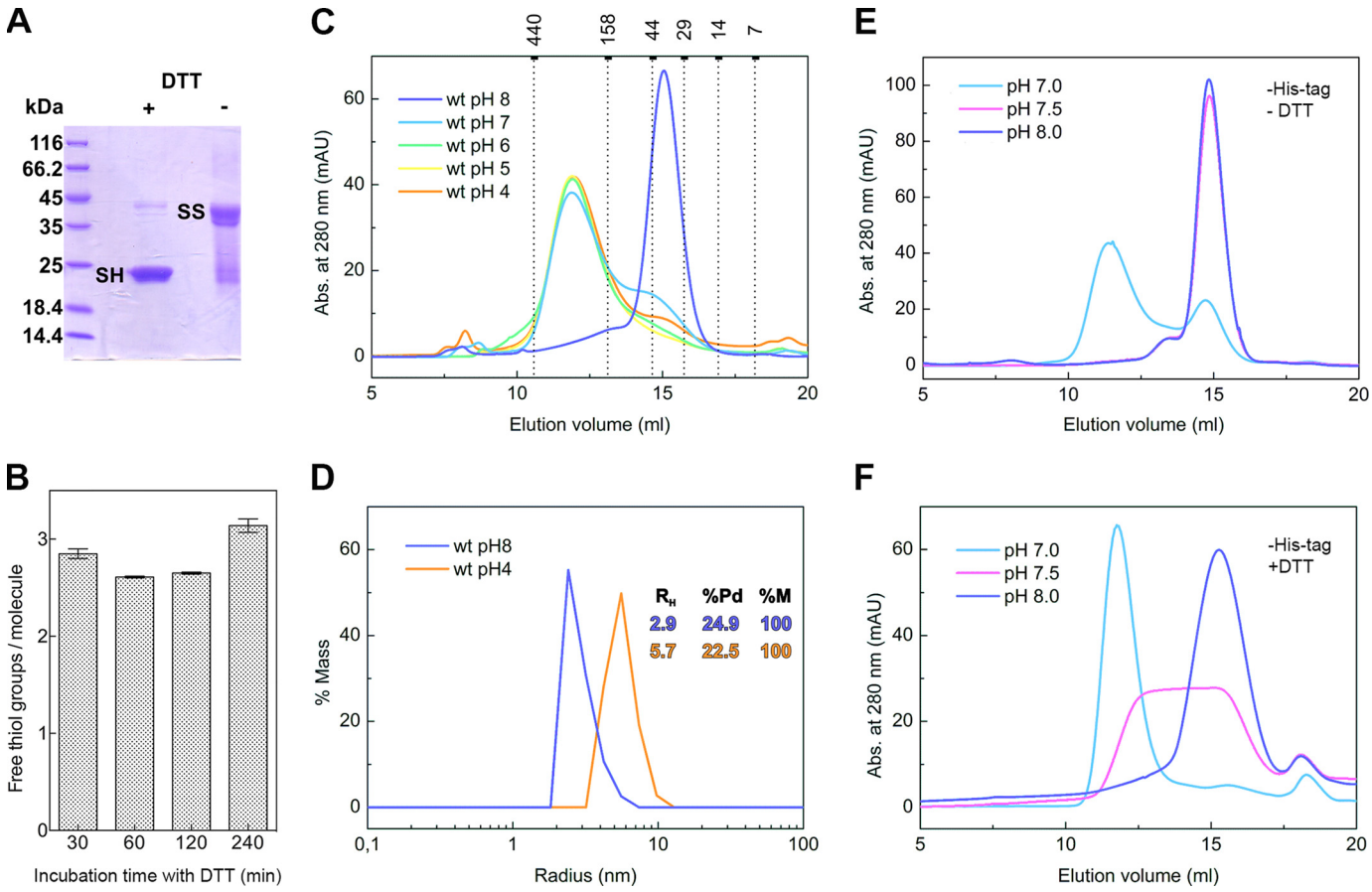

FIGURE 1. **Acidification shifts the dimer-decamer equilibrium to the decameric state.** *A*, SDS-PAGE under non-reducing conditions of *Lb*Prx1m samples (3 μg) showing reduced monomers (*SH*) upon pre-treatment with 2 mM DTT (+) and disulfide-bonded (*SS*) dimers in the absence of DTT (−). *B*, content of *Lb*Prx1m thiols determined by a DTNB assay with samples pre-treated with 2 mM DTT for 30, 60, 120, and 240 min. The values correspond to the calculated average of three independent experiments. *C*, SEC chromatograms of oxidized (*SS*) *Lb*Prx1m (wt) at 48 μM. The protein was pretreated with Chelex 100 (Bio-Rad) and loaded onto a column pre-equilibrated with 50 mM MMT (pH 4–8), 10 mM EDTA, and 150 mM NaCl. *Numbers above* the graphic represent the molecular masses (kDa) of standard proteins used for column calibration. *Gray dotted lines* indicate their respective elution volumes. *D*, DLS assays of oxidized *Lb*Prx1m (wt) at 48 μM in pH 4 and 8. R_H = hydrodynamic radius (nm), %Pd = polydispersity (%), %M = fraction of mass (%) corresponding to the peak. *E* and *F*, SEC chromatograms of TEV-cleaved *Lb*Prx1m at 48 μM under non-reducing conditions (*E*) and in the presence of 2 mM DTT (*F*) in 25 mM Tris-HCl buffer (pH 7.0, 7.5, and 8.0) containing 5 mM EDTA and 150 mM NaCl.

Thus, collectively, these data point out that *Lb*Prx1m dimer-decamer equilibrium is susceptible to small variations around physiological pH, being shifted to the decameric state upon acidification and to the dimeric state at mild basic conditions, regardless of whether C_P is reduced or disulfide bonded.

LbPrx1m Crystallized as a Dimer at Basic pH and as a Decamer at Acidic pH—In accordance with aSEC and DLS results, *LbPrx1m* crystals grown at pH 8.5 presented a dimer in the asymmetric unit, whereas those grown at pH 4.4 displayed a decamer. Energetic analyses using PDBePISA (42) confirmed that the dimer found in the asymmetric unit is the most stable assembly detected in the crystal, indicating the absence of higher order oligomers generated by symmetry.

The *Lb*Prx1m decamer is a doughnut-like structure formed by the association of five homodimers (Fig. 2). Each homodimer is stabilized by an anti-parallel intermolecular association between β7 strands from both subunits (Fig. 2*A*). This interface is named by Sarma and colleagues (43) as B-type interface (B for "β-sheet" based). To form the decamer, five B-type dimers interact each other via dimer-dimer interfaces named A-type (A for alternate or ancestral) (43) (Fig. 2*B*).

*Lb*Prx1m is oxidized in both crystal structures. In the dimeric crystalline form, the electronic density map allowed the modeling of the disulfide bond between Cys^{81} (C_P) from chain B and Cys^{204} (C_R) from chain A (Fig. 2, *A* and *C*). In the other active site, part of the catalytic loop (C_P-loop) and the whole C-terminal extension (after residue Asn^{198}) are disordered, probably due to a higher flexibility of this region. In all decamer subunits, the C_P-loop is well ordered and assumes a locally unfolded conformation, exposing C_P. The electron density map allowed the modeling of the disulfide bond of C_P from subunits A, C, and G with C_R from subunits B, D, and H, respectively (Fig. 2, *B* and *D*). In the remaining chains, the region from Asn^{198} to Asn^{225} is disordered. A similar pattern was already observed in the oxidized forms of Prx IV (44) and AcePrx-1 (45) and can be either due to inherent flexibility of C_R and adjacent residues or due to disulfide bond disruption by radiation damage during data collection.

His^{113} Is a pH Sensor for Decamerization—Comparison between the dimeric (pH 8.5) and decameric (pH 4.4) structures of *Lb*Prx1m showed that the C_P-loop is locally unfolded and undergoes conformational changes upon decamerization

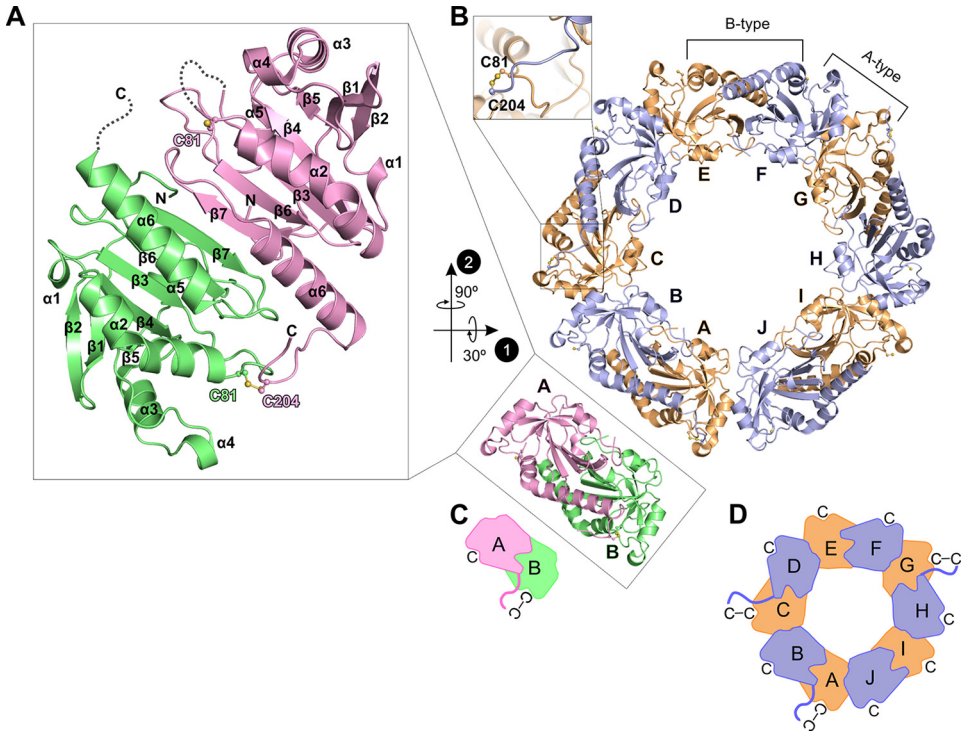

FIGURE 2. **Crystal structures of *Lb*Prx1m in dimeric and decameric forms.** *A*, schematic representation of the *Lb*Prx1m dimer crystallized at pH 8.5. Secondary structure elements are labeled and dimer subunits are colored in *pink* (chain A) and *green* (chain B). C_P (*C81*) and C_R (*C204*) are labeled and represented by ball-and-sticks. *Dotted lines* illustrate disordered regions absent from the crystallographic model. *B,* schematic representation of the *Lb*Prx1m decamer compared with the *Lb*Prx1m dimer. Decamer subunits are labeled (*A–J*) and the dimer interface (B-type) as well as the dimer-dimer interface (A-type) are highlighted. C_P and C_R are represented by ball and sticks. The *inset* shows an amplified view of the C_P-C_R disulfide bond at the C:D dimer. Schematic representations of dimer (*C*) and decamer (*D*) highlight the active sites where C_P-C_R bonds were observed (C-C) and the active sites where only C_P was modeled. In all cases, locally unfolded conformations were observed.

(Fig. 3, *A* and *B*). In the dimeric form, this loop assumes an open conformation that exposes to the surface the residues Asp^{76}, Asp^{108}, and Ser^{112} (Fig. 3*A*). Conversely, in the decameric form, an intramolecular hydrogen bond network involving Tyr^{73}, Asp^{76}, Ser^{106}, Asp^{108}, and Ser^{112}, as well as electrostatic interactions of His^{113} with Asp^{76}, locks the C_P-loop in a closed conformation (Fig. 3*B*). Upon this conformational change, Phe^{77} and Phe^{79} are placed at orientations that permit hydrophobic contacts with residues Ile^{55}, Tyr^{111}, Leu^{114}, and Ala^{115} from the adjacent subunit, favoring the decameric assembly (Fig. 3*B*). Among these residues, only His^{113} might have its protonation state affected in the pH interval where the dimer-to-decamer transition was observed. Changes in the His^{113} side chain protonation probably contribute with decamer stabilization through electrostatic interactions with Asp^{76} at pH below 8.0.

To test the hypothesis that His^{113} is relevant for the pH-induced decamerization of *Lb*Prx1m and evaluate the role of Asp^{76} in this process, we performed aSEC experiments with H113A and D76A mutants in the presence (pH 7) and absence (pH 4) of reducing agent (Fig. 3*C*). Samples treated with DTT were analyzed in neutral pH because the reducing power of DTT is lowered at acidic medium.

As expected, the H113A mutant eluted as a dimer in both conditions, demonstrating that *Lb*Prx1m depends on His^{113} to decamerize in neutral to acidic conditions regardless of whether C_P is reduced or disulfide bonded (Fig. 3*C*). The D76A mutant also eluted as a dimer when reduced and displayed two elution peaks when oxidized. DLS analysis of this sample indicated an average R_H of 3.5 nm and a polydispersity of 27%, supporting the predominance of D76A dimers observed in the aSEC profile (Fig. 3, *C* and *D*). Thus, aSEC and DLS data show that D76A substitution prevented the pH-induced decamerization of *Lb*Prx1m independent of the C_P redox state.

Together, these results indicate that the ionic interaction involving His^{113} and Asp^{76} side chains is pH-sensitive and crucial for decamerization upon acidification of *Lb*Prx1m in both reduced and disulfide-bonded states. Supporting this conclusion, the theoretical pK_a of His^{113} and Asp^{76} side chains in the decamer structure, calculated using the program PROPKA 3.0 (46), are 7.37 and 2.87, respectively, indicating that pH variations in the 7.0 to 8.0 interval might affect the protonation state of His^{113} and consequently the ionic interaction with the negatively charged Asp^{76}, which correlates with the dimer-to-decamer transition occurring in this pH range (Fig. 1*C*).

DISCUSSION

This work reveals that acidification in a narrow and physiological pH range favors the decamerization of both oxidized and reduced forms of *Lb*Prx1m, a typical 2-Cys Prx from protozoa. The same phenomenon has already been observed for oxidized forms of typical 2-Cys Prxs from plant and mammal (7, 21), but the structural basis for this pH effect was unknown so far.

Based on crystallographic, site-directed mutagenesis, and biophysical studies, we proposed a model to explain how pH modulates the dimer-decamer equilibrium of *Lb*Prx1m (Fig.

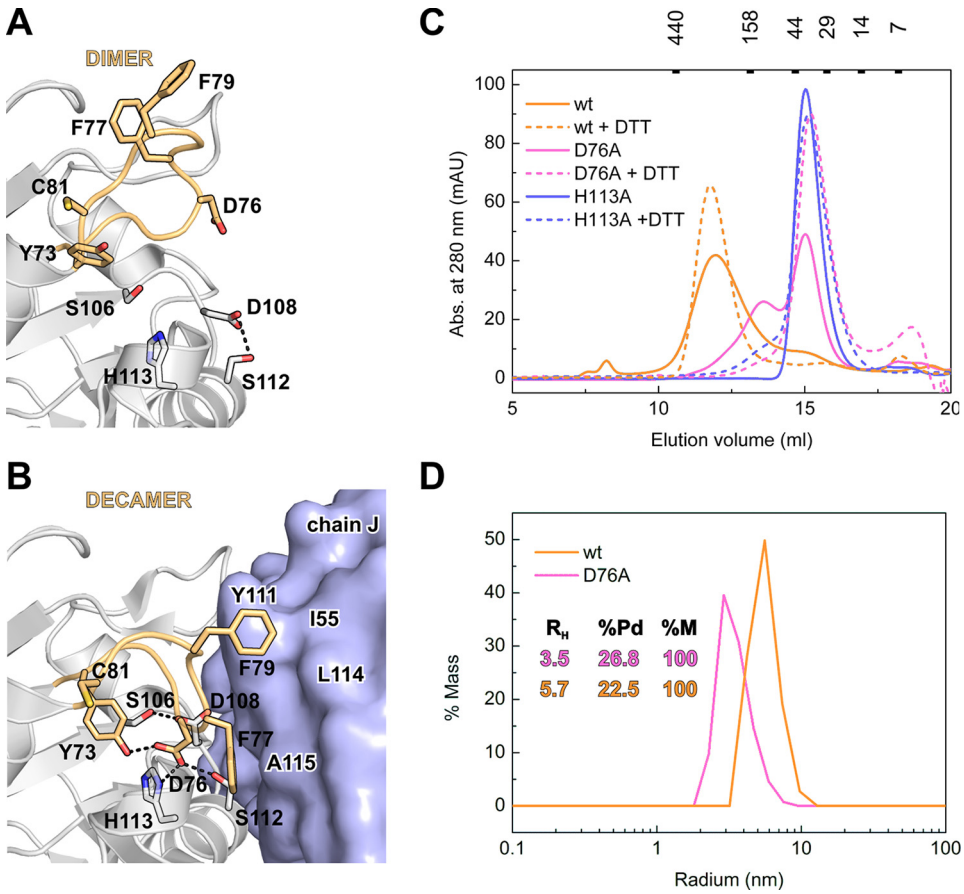

FIGURE 3. **Structural basis for the pH-induced decamerization of *Lb*Prx1m.** *Panels A* and *B* show a structural comparison between the active sites of *Lb*Prx1m dimer (*A*) and decamer (*B*) highlighting the C_P-loop (*light orange schematic*) and residues (*sticks*) involved in the decamerization process as well as C_P (Cys^{81}). For clarity purposes, the C_P-C_R disulfide bond was omitted in both structure representations. *Dashed lines* represent hydrogen bonds. *Labels outlined in white* indicate residues from the other subunit (*violet* surface, *panel B*) that compose the A-type interface. *C,* SEC chromatograms of *Lb*Prx1m at 48 μM (wt and mutants D76A (D76A) and H113A (H113A) under non-reducing (*solid lines*, 50 mM MMT, pH 4, 10 mM EDTA, and 150 mM NaCl) and reducing (*dashed lines*, 25 mM Tris-HCl, pH 7.0, 5 mM EDTA, 150 mM NaCl, and 2 mM DTT) conditions. *Numbers above* the graphic represent the molecular mass (kDa) of standard proteins used for column calibration. *D,* DLS assays of wt and the D76A mutant at 48 μM in 50 mM MMT (pH 4), 10 mM EDTA, and 150 mM NaCl. R_H = hydrodynamic radius (nm), %Pd = polydispersity (%), %M = fraction of mass (%) corresponding to the peak.

4A), in which the pH decrease triggers *Lb*Prx1m decamer formation by modulating the protonation state of His^{113}. As the pH decreases, His^{113} becomes positively charged and attracts Asp^{76}, located at the C_P-loop. This interaction induces a conformational change in the C_P-loop, locking it in a closed conformation and positioning Phe^{77} and Phe^{79} to create the A-type interface. As the pH increases, electrostatic interactions between His^{113} and Asp^{76} become weaker and *Lb*Prx1m decamers start to dissociate into dimers.

The His^{113} and Asp^{76} pair as well as other residues involved in the oligomerization of 2-Cys Prxs are highly conserved in Prx1 subfamily members, suggesting that the proposed padlock mechanism can be extended for most typical 2-Cys Prxs (Fig. 4*B*). Supporting this hypothesis, the position and orientation of Asp^{76} and His^{113} counterparts are fully conserved in homologous decamers, regardless the C_P redox state (Fig. 5). Moreover, the enzyme *Pf*Trx-Px2, which crystallized as an oxidized dimer at pH 6.5 (47), has an Asn replacing the corresponding Asp^{76}, suggesting that lack of the Asp-His ionic pair rendered its oligomerization pH-insensitive.

The dimer-to-decamer transition of *Lb*Prx1m, the human Prx II (21), and the chloroplast 2-Cys Prx from *Pisum sativum* (7) occur in a narrow pH range between pH 7 and 8, supporting that small variations of the physiological pH can have major effects in the dimer-decamer equilibrium of typical 2-Cys Prxs *in vivo*. It has been reported that pH variations regulate important cellular process, such as apoptosis in mammalian cells (48) and CO_2 fixation in plants (23). Apoptotic stimuli induce cytosol acidification, usually of 0.4 pH units (48), whereas the dark-light transition induces a rise in the chloroplast stromal pH from 7.0 to 8.0 (23). Mitochondrial pH can vary up to 0.5 pH units (basal pH ~ 8) in mammalian cells (22). According to our results (Fig. 1) and other studies (7, 21), the dimer-decamer equilibrium of Prx1 members is responsive to such pH variations, suggesting that changes in pH homeostasis can influence the quaternary structure of cytosolic, mitochondrial, and chloroplast Prx1 members such as the human Prx II, *Lb*Prx1m, and pea 2-Cys Prx, respectively.

The pH effect on the oligomerization of typical 2-Cys Prxs supports the hypothesis that intracellular pH affects mechanisms controlling the cellular concentration of reactive oxygen species (48). Changes in the oligomeric state of these enzymes influence both the peroxidase activity and the functional switch. The decameric form stabilizes the FF conformation

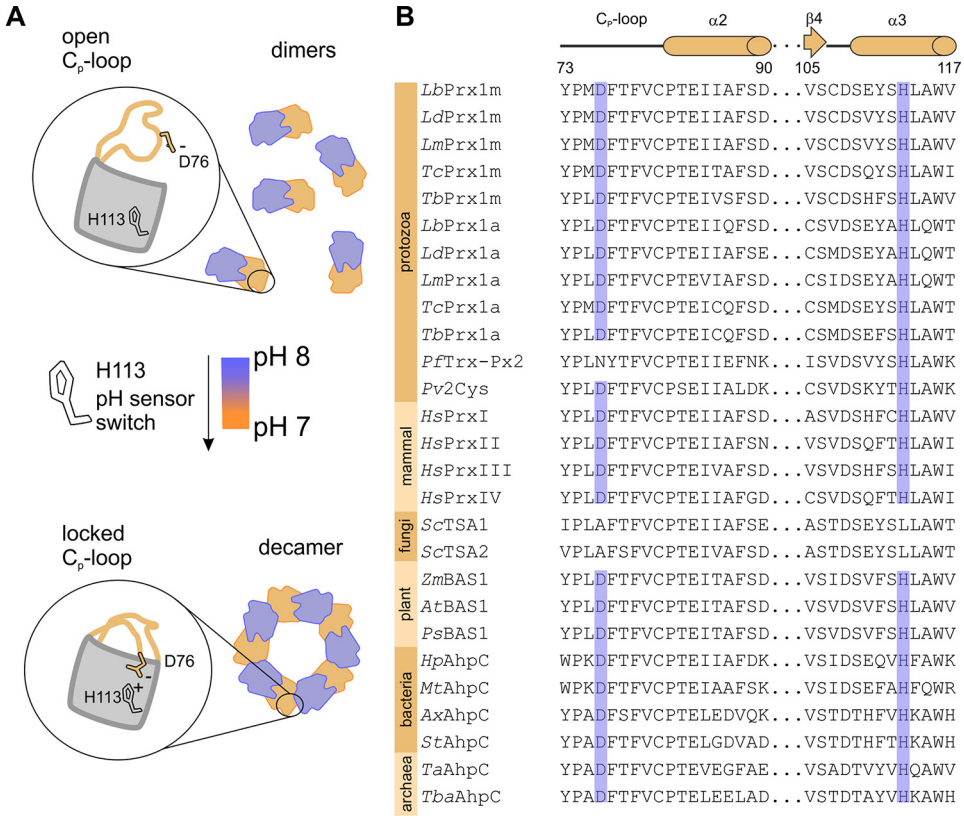

FIGURE 4. **The padlock model proposed for the pH-induced decamerization of *Lb*Prx1m.** *A*, in this model, His^{113} functions as a pH sensor switch. With decreasing pH, His^{113} becomes protonated and attracts the residue Asp^{76}, inducing the C_P-loop to change from an open to a closed conformation that promotes the decamerization. *B*, sequence alignment of Prx1 subfamily members from divergent phylogenetic groups. Species abbreviations are as follows: *Lb, L. braziliensis; Ld, Leishmania donovani; Lm, Leishmania major; Tc, Trypanosoma cruzi; Tb, T. brucei; Pf, Plasmodium falciparum; Pv, P. vivax; Hs, Homo sapiens; Sc, Saccharomyces cerevisiae; Zm, Zea mays; At, Arabdopsis thaliana; Ps, P. sativum; Hp, Helicobacter pylori; Mt, Mycobacterium tuberculosis; Ax, Amphibacillus xylanus; St, Salmonella typhimurium; Ta, Thermoplasma acidophilum; Tba, Thermococcus barophilus*. Conserved residues Asp^{76} and His^{113} (*Lb*Prx1m numbering) are highlighted in *violet*.

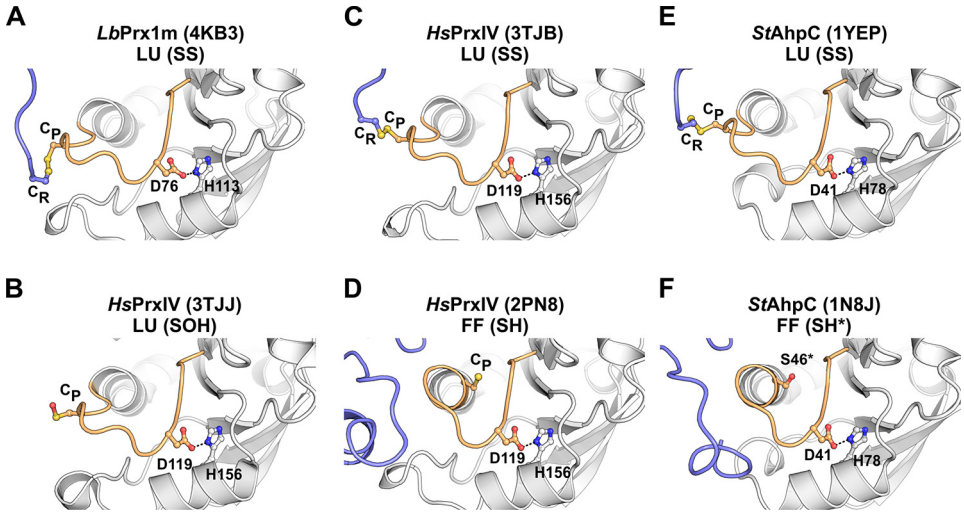

FIGURE 5. **The structural conservation of the Asp^{76}-His^{113} interaction in decamers of Prx1 subfamily.** Structural comparisons between *Lb*Prx1m and homologous decamers with C_P in sulfenylated (*SOH*), disulfide-bonded (*SS*), and reduced (*SH*) states revealed that the positions of Asp^{76} and His^{113} counterparts (*sticks*) are fully conserved and compatible with the formation of an ionic interaction between their side chains. All structures are presented in the same orientation (*A–F*). The C_P-loop and the C-terminal of the neighbor subunit forming the active site are highlighted in *light orange* and *violet*, respectively. *Dashed lines* indicate inter-atomic distances of 2.4–2.6 Å. PDB codes are presented in *parentheses* after the protein names (abbreviated as in Fig. 4). For clarity purposes, one alternative conformation of the C_P side chain from 3TJJ was omitted and the side chain of His^{78} from PDB 1N8J was flipped as suggested by Molprobity analysis (40). *, C46S mutant mimics the C_P reduced state (*SH**). *FF*, fully folded conformation. *LU*, locally unfolded conformation.

required for the nucleophilic attack of the C_P thiolate on the peroxide substrate, rendering the sulfenylation (C_P-SOH) and eventually the overoxidation of C_P (3). Supporting this idea, 2-Cys Prx mutants unable to decamerize display lower catalytic efficiency and are less responsive to peroxide-mediated inactivation (49). Upon the disulfide bond formation between

C_P-SOH and C_R-SH, Prx1 subfamily decamers tend to dissociate into dimers, a process that seems to be important for the recycling step by another protein or small molecule thiol (20). For instance, recycling of rat Prx I by reduced thioredoxin is more efficient when the protein is in the dimeric state (20).

In light of these evidences and considering our findings, we suggest that pH-induced decamerization may have a dual effect depending on the redox state of the Prx1 species. By stabilizing reduced (SH) decamers, acidification probably boosts the peroxidation step of the catalytic cycle. On the other hand, by stabilizing oxidized (SS) decamers, it might hinder the recycling step, decreasing the conversion rate of SS to SH forms. An inefficient recycling step has been associated with a lower frequency of C_P overoxidation (44). The latter process has been implicated in H_2O_2 signal transduction (50) and was associated with a peroxidase-to-chaperone switch (11, 12), suggesting that the pH effect on enzyme oligomerization may influence H_2O_2 signaling pathways and the cell response to oxidative stress. Despite the redox state being considered the major driving force for decamer-dimer transition, our results demonstrated that pH changes in a narrow physiological range can also be a key factor in this event. Therefore, more studies are required to shed light on how the redox state cross-talks with other oligomerization-modulating factors such as pH to regulate the structure and function of Prx1 subfamily members *in vivo*.

Acknowledgments—We are grateful to the Brazilian Biosciences National Laboratory (LNBio) and the Brazilian Synchrotron Light Laboratory (LNLS) for the provision of time on the MX2 and SAXS2 beamlines, ROBOLAB, LPP, and LEC.

REFERENCES

1. Winterbourn, C. C. (2008) Reconciling the chemistry and biology of reactive oxygen species. *Nat. Chem. Biol.* **4,** 278–286
2. Nelson, K. J., Knutson, S. T., Soito, L., Klomsiri, C., Poole, L. B., and Fetrow, J. S. (2011) Analysis of the peroxiredoxin family: using active-site structure and sequence information for global classification and residue analysis. *Proteins* **79,** 947–964
3. Hall, A., Nelson, K., Poole, L. B., and Karplus, P. A. (2011) Structure-based insights into the catalytic power and conformational dexterity of peroxiredoxins. *Antioxid. Redox. Signal.* **15,** 795–815
4. Castro, H., Sousa, C., Santos, M., Cordeiro-da-Silva, A., Flohé, L., and Tomás, A. M. (2002) Complementary antioxidant defense by cytoplasmic and mitochondrial peroxiredoxins in Leishmania infantum. *Free Radic. Biol. Med.* **33,** 1552–1562
5. Aran, M., Ferrero, D. S., Pagano, E., and Wolosiuk, R. A. (2009) Typical 2-Cys peroxiredoxins: modulation by covalent transformations and noncovalent interactions. *FEBS J.* **276,** 2478–2493
6. Chang, T. S., Cho, C. S., Park, S., Yu, S., Kang, S. W., and Rhee, S. G. (2004) Peroxiredoxin III, a mitochondrion-specific peroxidase, regulates apoptotic signaling by mitochondria. *J. Biol. Chem.* **279,** 41975–41984
7. Bernier-Villamor, L., Navarro, E., Sevilla, F., and Lázaro, J. J. (2004) Cloning and characterization of a 2-Cys peroxiredoxin from *Pisum sativum*. *J. Exp. Bot.* **55,** 2191–2199
8. Tavender, T. J., Sheppard, A. M., and Bulleid, N. J. (2008) Peroxiredoxin IV is an endoplasmic reticulum-localized enzyme forming oligomeric complexes in human cells. *Biochem. J.* **411,** 191–199
9. Wood, Z. A., Schröder, E., Robin Harris, J., and Poole, L. B. (2003) Structure, mechanism and regulation of peroxiredoxins. *Trends Biochem. Sci.* **28,** 32–40
10. Wood, Z. A., Poole, L. B., Hantgan, R. R., and Karplus, P. A. (2002) Dimers to doughnuts: redox-sensitive oligomerization of 2-cysteine peroxiredoxins. *Biochemistry* **41,** 5493–5504
11. Jang, H. H., Lee, K. O., Chi, Y. H., Jung, B. G., Park, S. K., Park, J. H., Lee, J. R., Lee, S. S., Moon, J. C., Yun, J. W., Choi, Y. O., Kim, W. Y., Kang, J. S., Cheong, G. W., Yun, D. J., Rhee, S. G., Cho, M. J., and Lee, S. Y. (2004) Two enzymes in one: two yeast peroxiredoxins display oxidative stress-dependent switching from a peroxidase to a molecular chaperone function. *Cell* **117,** 625–635
12. Moon, J. C., Hah, Y. S., Kim, W. Y., Jung, B. G., Jang, H. H., Lee, J. R., Kim, S. Y., Lee, Y. M., Jeon, M. G., Kim, C. W., Cho, M. J., and Lee, S. Y. (2005) Oxidative stress-dependent structural and functional switching of a human 2-Cys peroxiredoxin isotype II that enhances HeLa cell resistance to H2O2-induced cell death. *J. Biol. Chem.* **280,** 28775–28784
13. Guimarães, B. G., Souchon, H., Honoré, N., Saint-Joanis, B., Brosch, R., Shepard, W., Cole, S. T., and Alzari, P. M. (2005) Structure and mechanism of the alkyl hydroperoxidase AhpC, a key element of the *Mycobacterium tuberculosis* defense system against oxidative stress. *J. Biol. Chem.* **280,** 25735–25742
14. Chuang, M. H., Wu, M. S., Lo, W. L., Lin, J. T., Wong, C. H., and Chiou, S. H. (2006) The antioxidant protein alkylhydroperoxide reductase of *Helicobacter pylori* switches from a peroxide reductase to a molecular chaperone function. *Proc. Natl. Acad. Sci. U.S.A.* **103,** 2552–2557
15. Barranco-Medina, S., Lázaro, J. J., and Dietz, K. J. (2009) The oligomeric conformation of peroxiredoxins links redox state to function. *FEBS Lett.* **583,** 1809–1816
16. Jang, H. H., Kim, S. Y., Park, S. K., Jeon, H. S., Lee, Y. M., Jung, J. H., Lee, S. Y., Chae, H. B., Jung, Y. J., Lee, K. O., Lim, C. O., Chung, W. S., Bahk, J. D., Yun, D. J., Cho, M. J., and Lee, S. Y. (2006) Phosphorylation and concomitant structural changes in human 2-Cys peroxiredoxin isotype I differentially regulate its peroxidase and molecular chaperone functions. *FEBS Lett.* **580,** 351–355
17. Park, J. W., Piszczek, G., Rhee, S. G., and Chock, P. B. (2011) Glutathionylation of peroxiredoxin I induces decamer to dimers dissociation with concomitant loss of chaperone activity. *Biochemistry* **50,** 3204–3210
18. Engelman, R., Weisman-Shomer, P., Ziv, T., Xu, J., Arnér, E. S., and Benhar, M. (2013) Multilevel regulation of 2-Cys peroxiredoxin reaction cycle by *S*-nitrosylation. *J. Biol. Chem.* **288,** 11312–11324
19. Kitano, K., Niimura, Y., Nishiyama, Y., and Miki, K. (1999) Stimulation of peroxidase activity by decamerization related to ionic strength: AhpC protein from *Amphibacillus xylanus*. *J. Biochem.* **126,** 313–319
20. Matsumura, T., Okamoto, K., Iwahara, S., Hori, H., Takahashi, Y., Nishino, T., and Abe, Y. (2008) Dimer-oligomer interconversion of wild-type and mutant rat 2-Cys peroxiredoxin: disulfide formation at dimer-dimer interfaces is not essential for decamerization. *J. Biol. Chem.* **283,** 284–293
21. Kristensen, P., Rasmussen, D. E., and Kristensen, B. I. (1999) Properties of thiol-specific antioxidant protein or calpromotin in solution. *Biochem. Biophys. Res. Commun.* **262,** 127–131
22. Santo-Domingo, J., and Demaurex, N. (2012) Perspectives on: SGP symposium on mitochondrial physiology and medicine: the renaissance of mitochondrial pH. *J. Gen. Physiol.* **139,** 415–423
23. Werdan, K., Heldt, H. W., and Milovancev, M. (1975) The role of pH in the regulation of carbon fixation in the chloroplast stroma. Studies on CO_2 fixation in the light and dark. *Biochim. Biophys. Acta* **396,** 276–292
24. Matsuyama, S., Llopis, J., Deveraux, Q. L., Tsien, R. Y., and Reed, J. C. (2000) Changes in intramitochondrial and cytosolic pH: early events that modulate caspase activation during apoptosis. *Nat. Cell Biol.* **2,** 318–325
25. Gretes, M. C., Poole, L. B., and Karplus, P. A. (2012) Peroxiredoxins in parasites. *Antioxid. Redox Signal.* **17,** 608–633
26. Harder, S., Bente, M., Isermann, K., and Bruchhaus, I. (2006) Expression of a mitochondrial peroxiredoxin prevents programmed cell death in *Leishmania donovani*. *Eukaryot. Cell* **5,** 861–870
27. Carnielli, J. B., de Andrade, H. M., Pires, S. F., Chapeaurouge, A. D., Perales, J., Monti-Rocha, R., Carvalho, S. F., Ribeiro, L. P., Dietze, R., Figueiredo, S. G., and Lemos, E. M. (2014) Proteomic analysis of the soluble proteomes of miltefosine-sensitive and -resistant *Leishmania infantum chagasi* isolates obtained from Brazilian patients with different treatment outcomes. *J. Proteomics* **108,** 198–208
28. Dorlo, T. P., Balasegaram, M., Beijnen, J. H., and de Vries, P. J. (2012)

Miltefosine: a review of its pharmacology and therapeutic efficacy in the treatment of leishmaniasis. *J. Antimicrob. Chemother.* **67,** 2576–2597
29. Castro, H., Teixeira, F., Romao, S., Santos, M., Cruz, T., Flórido, M., Appelberg, R., Oliveira, P., Ferreira-da-Silva, F., and Tomás, A. M. (2011) *Leishmania* mitochondrial peroxiredoxin plays a crucial peroxidase-unrelated role during infection: insight into its novel chaperone activity. *PLoS Pathog.* **7,** e1002325
30. de Morais, M. A., de Souza, Tde A., and Murakami, M. T. (2013) Cloning, expression, purification, crystallization and preliminary x-ray diffraction analysis of the mitochondrial tryparedoxin peroxidase from *Leishmania braziliensis*. *Acta Crystallogr. Sect. F Struct. Biol. Cryst. Commun.* **69,** 408–411
31. Otwinowski, Z., and Minor, W. (1997) Processing of x-ray diffraction data collected in oscillation mode. *Macromol. Crystallogr. A* **276,** 307–326
32. Kabsch, W. (2010) *XDS*. *Acta Crystallogr. D Biol. Crystallogr.* **66,** 125–132
33. Vagin, A., and Teplyakov, A. (1997) MOLREP: an automated program for molecular replacement. *J. Appl. Crystallogr.* **30,** 1022–1025
34. McCoy, A. J., Grosse-Kunstleve, R. W., Adams, P. D., Winn, M. D., Storoni, L. C., and Read, R. J. (2007) Phaser crystallographic software. *J. Appl. Crystallogr.* **40,** 658–674
35. Terwilliger, T. C., Grosse-Kunstleve, R. W., Afonine, P. V., Moriarty, N. W., Zwart, P. H., Hung, L. W., Read, R. J., and Adams, P. D. (2008) Iterative model building, structure refinement and density modification with the PHENIX AutoBuild wizard. *Acta Crystallogr. D Biol. Crystallogr.* **64,** 61–69
36. Murshudov, G. N., Vagin, A. A., and Dodson, E. J. (1997) Refinement of macromolecular structures by the maximum-likelihood method. *Acta Crystallogr. D Biol. Crystallogr.* **53,** 240–255
37. Afonine, P. V., Grosse-Kunstleve, R. W., Echols, N., Headd, J. J., Moriarty, N. W., Mustyakimov, M., Terwilliger, T. C., Urzhumtsev, A., Zwart, P. H., and Adams, P. D. (2012) Towards automated crystallographic structure refinement with phenix.refine. *Acta Crystallogr. D Biol. Crystallogr.* **68,** 352–367
38. Emsley, P., and Cowtan, K. (2004) Coot: model-building tools for molecular graphics. *Acta Crystallogr. D Biol. Crystallogr.* **60,** 2126–2132
39. Painter, J., and Merritt, E. A. (2006) Optimal description of a protein structure in terms of multiple groups undergoing TLS motion. *Acta Crystallogr. D Biol. Crystallogr.* **62,** 439–450
40. Chen, V. B., Arendall, W. B., 3rd, Headd, J. J., Keedy, D. A., Immormino, R. M., Kapral, G. J., Murray, L. W., Richardson, J. S., and Richardson, D. C. (2010) MolProbity: all-atom structure validation for macromolecular crystallography. *Acta Crystallogr. D Biol. Crystallogr.* **66,** 12–21
41. Cao, Z., Bhella, D., and Lindsay, J. G. (2007) Reconstitution of the mitochondrial PrxIII antioxidant defence pathway: general properties and factors affecting PrxIII activity and oligomeric state. *J. Mol. Biol.* **372,** 1022–1033
42. Krissinel, E., and Henrick, K. (2007) Inference of macromolecular assemblies from crystalline state. *J. Mol. Biol.* **372,** 774–797
43. Sarma, G. N., Nickel, C., Rahlfs, S., Fischer, M., Becker, K., and Karplus, P. A. (2005) Crystal structure of a novel *Plasmodium falciparum* 1-Cys peroxiredoxin. *J. Mol. Biol.* **346,** 1021–1034
44. Cao, Z., Tavender, T. J., Roszak, A. W., Cogdell, R. J., and Bulleid, N. J. (2011) Crystal structure of reduced and of oxidized peroxiredoxin IV enzyme reveals a stable oxidized decamer and a non-disulfide-bonded intermediate in the catalytic cycle. *J. Biol. Chem.* **286,** 42257–42266
45. Nguyen, J. B., Pool, C. D., Wong, C. Y., Treger, R. S., Williams, D. L., Cappello, M., Lea, W. A., Simeonov, A., Vermeire, J. J., and Modis, Y. (2013) Peroxiredoxin-1 from the human hookworm *Ancylostoma ceylanicum* forms a stable oxidized decamer and is covalently inhibited by conoidin A. *Chem. Biol.* **20,** 991–1001
46. Li, H., Robertson, A. D., and Jensen, J. H. (2005) Very fast empirical prediction and rationalization of protein pK_a values. *Proteins* **61,** 704–721
47. Boucher, I. W., McMillan, P. J., Gabrielsen, M., Akerman, S. E., Brannigan, J. A., Schnick, C., Brzozowski, A. M., Wilkinson, A. J., and Müller, S. (2006) Structural and biochemical characterization of a mitochondrial peroxiredoxin from *Plasmodium falciparum*. *Mol. Microbiol.* **61,** 948–959
48. Lagadic-Gossmann, D., Huc, L., and Lecureur, V. (2004) Alterations of intracellular pH homeostasis in apoptosis: origins and roles. *Cell Death Differ.* **11,** 953–961
49. Parsonage, D., Youngblood, D. S., Sarma, G. N., Wood, Z. A., Karplus, P. A., and Poole, L. B. (2005) Analysis of the link between enzymatic activity and oligomeric state in AhpC, a bacterial peroxiredoxin. *Biochemistry* **44,** 10583–10592
50. Wood, Z. A., Poole, L. B., and Karplus, P. A. (2003) Peroxiredoxin evolution and the regulation of hydrogen peroxide signaling. *Science* **300,** 650–653
51. Karplus, P. A., and Diederichs, K. (2012) Linking crystallographic model and data quality. *Science* **336,** 1030–1033

How pH Modulates the Dimer-Decamer Interconversion of 2-Cys Peroxiredoxins from the Prx1 Subfamily

Mariana A. B. Morais, Priscila O. Giuseppe, Tatiana A. C. B. Souza, Thiago G. P. Alegria, Marcos A. Oliveira, Luis E. S. Netto and Mario T. Murakami

J. Biol. Chem. 2015, 290:8582-8590.
doi: 10.1074/jbc.M114.619205 originally published online February 9, 2015
